Proceedings of the ASME 2010 3rd Joint US-European Fluids Engineering Summer Meeting and 8th International Conference on Nanochannels, Microchannels, and Minichannels
FEDSM-ICNMM2010
August 1-5, 2010, Montreal, Canada

FEDSM-ICNMM2010-30412

Optothermal Control of Local Fluid Temperature in Microfluidics

M. Akbari
Mechatronic System Engineering School of Engineering Science, Simon Fraser University, Surrey, BC, V3T 0A3, Canada.

M. Bahrami
Mechatronic System Engineering School of Engineering Science, Simon Fraser University, Surrey, BC, V3T 0A3, Canada.

D. Sinton
Department of Mechanical Engineering, University of Victoria,Victoria, BC, V8W 2Y2, Canada.

ABSTRACT

This paper outlines an optothermal approach to manipulate local fluid temperatures in microfluidic and lab-on-chip systems. The system has the ability to control the size, location and the source heat flux using an external computer and is not constrained by predefined geometries, complex fabrication or control system. The thermal performance is evaluated using a temperature-dependent fluorescent dye. Experiments demonstrate localized heating up to 35℃ over ambient temperature for a heat source spanning a downstream length of 1.5 mm. Experimental results are compared with a 1D thermal analysis of the system based on the Taylor-Aris dispersion.

NOMENCLATURE

A = Cross-sectional area, m^2
Bi = Biot number, $(hl^2/2Hk)(\alpha/\alpha_{eff})$
c_p = Minimum width of the hyperbolic contraction, m
h = Convective/conductive heat transfer coefficient, $W/m^2.K$
H = Channel half height, m
k = Fluid thermal conductivity, $W/m.K$
l = Heat source width, m
L = Channel half length, m
Q_{pd} = Pressure driven flow rate, m^3/s
Pe_l = Peclet number, $\bar{u}l/\alpha_{eff}$
Pe_H = Peclet number, $Pe_H = \bar{u}H(1 - u_{eo,0}fg/\bar{u})/\alpha$

Greek
$\boldsymbol{\alpha}$ = Thermal diffusivity, $\mathbf{m^2/s}$
$\boldsymbol{\alpha_{eff}}$ = Dispersion coefficient, $\mathbf{m^2/s}$
$\boldsymbol{\Delta V}$ = Applied voltage, $\mathbf{V}$
$\boldsymbol{\eta}$ = Fluid viscosity, $\mathbf{Pa.s}$
$\boldsymbol{\mu_{eo}}$ = Electroosmotic mobility, $\mathbf{m^2/V.s}$

1. INTRODUCTION

Improved temperature control was one of the main motivating factors for some of the earliest microfluidic chip based systems Active control of fluid temperatures is now central to many microfluidic and lab on chip applications. Examples include chemical synthesis in microreactors [1, 2], polymerase chain reaction (PCR) (see ref. [3] for a comprehensive review), pre-concentration and separation techniques [4, 5], and optothermal flow manipulation [6-8]. In particular, localized on-chip temperature variations are employed in patch-clamp electrophysiology [2], rheological flow manipulation [7], polymer actuators [8], and to separate analytes [4].

In present technologies, the following methods have been applied to provide heating for microdevices: thin-film heating elements made of Pt, Ti, and nonmetallic polysilicon [9-11], heating by embedded resistance wires or silver-filled epoxy [12, 20], external Peltier modules [4, 13], heating by hot air [14,15], heating by infra red or halogen light or microwave [16-

18], chemical reaction heating [19], laser heating [6, 7], and joule heating [5,21].

Use of an integrated electrical heater is one of the most common methods for on-chip temperature control [12], however, the heating structures must to be designed, fabricated, and integrated within the microchip, and the location of the heated zones cannot be changed dynamically. The fabrication of integrated heaters is also fairly complex (such as patterning multilayer soft-lithography systems or on-chip heaters), and the heaters must be interfaced with the external environment (e.g. electrical connections).

Limitations associated with fixed on-chip electrical heaters has motivated the development of non-contact heating approaches; particularly optothermal heating methods. Using suspended photothermal nanoparticles and submiliwatt light beams, Liu et al. [22] proposed a contactless fluid manipulation system to transport biomolecules and living cells at controlled speeds and directions. Reinhardt et al. [23], presented a μ-hotplate enhanced optical heating system by fabrication of microsized patterned surfaces for single cell treatment. Krishnan et al. [7] demonstrated a microfluidic valving technique based on optothermorheological manipulation using a low-power laser beam. Their system is able to generate reversible valves with the switching times on the order of $1\ s$ at high flow rates of $1\ mm/s$. Richter and Paschew [8], developed a highly integrated polymer-based actuation system using a stimuli-responsive hydrogel. Activation of the actuators was implemented by optical system including a commercial video projector and convex lenses.

In this work, we use a commercial video projector and an optical setup to achieve optothermal heating of an aqueous solution in a microfluidic channel. This method presents improved flexibility over integrated heaters, and can produce localized heating and simultaneous heat sources at multiple locations. The thermal characteristics of the heating system were measured by using the temperature-dependent fluorescent dye method [30]. A 1D approach for thermal analysis of the system is also provided for better understanding of the heat transfer and temperature distribution along the microchannel. This analytical approach can be implemented to other heating techniques that produce localized heating.

2. EXPERIMENTAL SECTION

Temperature sensitive rhodamine B dye (Sigma Aldrish, St. Louis, Missouri) was used for the temperature measurements. In our experiments, an inverted epi-fluorescent microscope (Jenco, Oregon) with 5X, 0.12 N.A. long distance objective, a rhodamine B filter set (excitation: band pass 546 nm/12 nm, emission: band pass 600 nm/40 nm), a broadband mercury illumination source, and a digital CCD camera was used. Image acquisition and storage was controlled by the Zarbco video toolbox (Ver. 1.65) software. Hydrostatic pressure (i.e. difference between two columns of water) was used to produce ultra-small flow rates of $Q < 10\mu L/hr$ while a syringe pump (Harvard Apparatus, QC, Canada) was used to produce higher flow rates (up to $1500\mu L/hr$). The range of the Reynolds number for this experiment varied between 0.005 to 5; ensures the laminar flow. A commercial video projector (Sony, 3-LDC BrightEra, 190 W Mercury lamp, 1600/2000 ANSI lumens) equipped with special optics consisting of three convex lenses were used for optothermic control of the system. A 50 mm long rectangular borosilicate glass capillary (Vitrocom, NJ) with nominal inner dimensions of $20 \times 200\ \mu m$ was used as the microchannel. Two different materials of Poly (methyl methacrylate) (PMMA) and glass (both with the dimensions of $25\ mm \times 75mm \times 1mm$) were employed to mount the capillaries. A microscope slide were used as the glass substrate while the PMMA substrate was produced using a CO_2 laser system. A black electric tape is fixed on the surface of the microchannel, providing a light absorbing material. Images were projected onto the surface of the black tape using the abovementioned optical setup and the user interface software of Microsoft Power Point. Polydimethyl siloxane (PDMS) layers were punched and used at the channel ends to interface the external fluidics. The microfluidics assembly and a schematic of the experimental setup are shown in Figure 1.

Prior to each experiment a background and an isothermal "cold field" intensity image of the system were taken. Following the acquisition of the cold field image, the prescribed flow rate was set and a rectangular strip of light is projected onto the surface of the black tape to provide localized heating. The heat source width was estimated to be 1.5 mm. Images were taken every 2 min with the resolution of 1280×1024 pixels, which captured a length of 3.5 mm of the channel. The system was considered to have reached the steady-state condition when the measured temperature distribution did not change with time. In order to avoid the photobleaching effect and channel heating due to the high intensity illumination light, images were recorded for periods of less than 5 seconds [24].

To extract the in-channel temperature profiles, background image was first subtracted from each raw image and the cold field. The corrected raw images were then normalized with the corrected cold field images. A Wiener type adaptive filter was then applied in order to smooth the images and reduce the effect of noise. The intensity values of the treated images were then converted to temperature using the intensity vs. temperature calibration, as described by [21].

3. THEORETICAL MODEL

In this section, we present a simple approach for better understanding of the heat transfer and temperature distribution along the microchannel for the proposed optothermal heating method. It should be noted that the proposed theoretical model can also be implemented to other heating techniques such as thin film heating and heating via resistance wire with appropriate modifications.

We model our thermal system using a convection-diffusion heat transfer equation for a microchannel shown in Figure 2, with the following assumptions:

- steady-state heat transfer and fluid flow

- thermal properties are constant
- channel is long enough that the inlet and outlet effects on the temperature distribution can be neglected
- fluid temperature is room temperature at the inlet and outlet
- flow is 2D (channel is sufficiently wide)
- flow is stokes flow (low Re) (see [25 and 26] for more details)
- joule heating effect is negligible

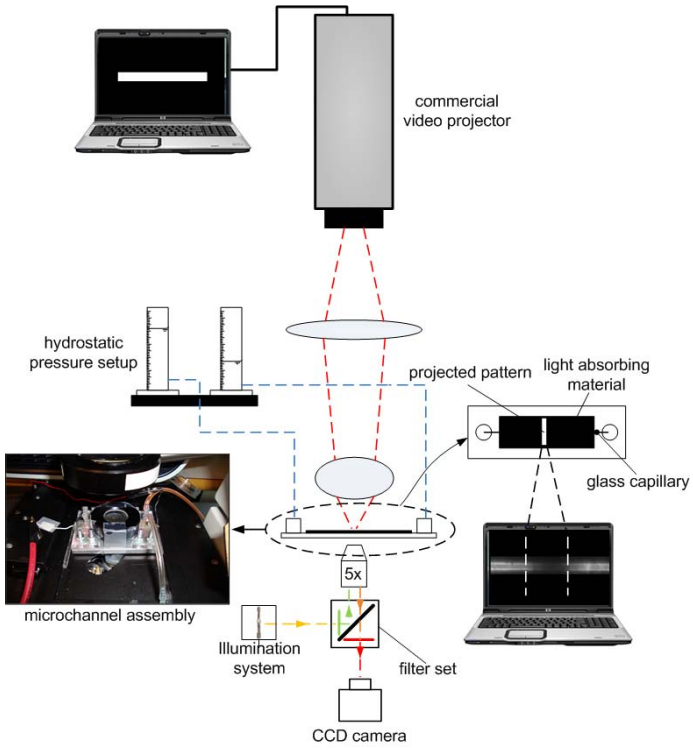

Figure 1. Sc hematic of t he e xperimental s etup a nd microchip assembly. No te that for hi gh f low rates a s yringe p ump is used instead of the hydrostatic flow setup.

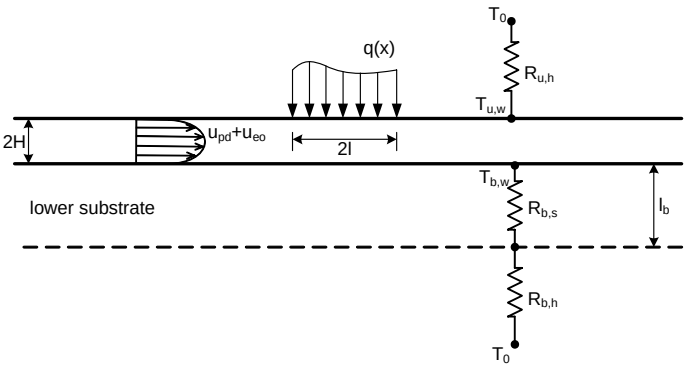

Figure 2. Sch ematic o f the hea ted micr ochannel a nd it s 1-D resistance network.

For such a model system, the conservation of energy can be written as follows

$$u\frac{\partial\theta}{\partial x}=\alpha\left(\frac{\partial^2\theta}{\partial x^2}+\frac{\partial^2\theta}{\partial y^2}\right) \tag{1}$$

holding the following boundary conditions

$$\left.\frac{\partial\theta}{\partial y}\right|_{y=H}=\frac{q_u(x)}{k}$$

$$\left.\frac{\partial\theta}{\partial y}\right|_{y=-H}=\frac{q_b(x)}{k} \tag{2}$$

$$\theta|_{x=\pm L}=0$$

where $\theta=T-T_0$ is the temperature rise, T_0 is the reference temperature (here room temperature), u_{bulk} is the bulk velocity which is the summation of pressure driven velocity, u_{pd} and electroosmotic velocity, u_{eo}, H is the channel half-height, l is the channel half-length, k is the thermal conductivity, $\alpha=k/\rho c_p$ is the thermal diffusivity, and $q_u(x)$ and $q_b(x)$ are the heat fluxes of the upper and lower wall boundary conditions. Note that the proposed approach is valid for boundary conditions including convective, radiative, or constant temperature.

In most microchannel systems, the Reynolds number is much less than unity and the Debye length is several orders of magnitude smaller than the characteristic dimensions of the channel. Using the lubrication flow solution of Ghosal [25] to include variable viscosity and the nonuniform electroosmotic slip velocity, the following relationship is obtained by Huber and Santiago (for more details see the appendix of Ref [26]) for the bulk velocity

$$u(x,y)=\left\{\frac{Q_{pd}}{H}+\frac{3}{2}\frac{\mu_{eo,0}\Delta V}{L}\left(\frac{\langle\eta f g\rangle}{\langle\eta\rangle}-fg\right)\right\}\left(1-\frac{y^2}{H^2}\right) \tag{3}$$

where Q_{pd} is the pressure driven flow rate, η is the fluid viscosity, $\mu_{eo,0}$ is the electroosmotic mobility of the fluid at a reference temperature (usually room temperature), and ΔV is the applied voltage. The $f(T)$ in Eq. (3) is a nondimensional function accounts for any other temperature dependence of the buffer electrical conductivity which is not through the viscosity [4]. We also used the same definition used by Huber and Santiago [26] for $g(T)=\mu_{eo}(T)\eta(T)/\mu_{eo,0}\eta_0$. Note that the axial averaging used in the lubrication solution [25] is denoted by $\langle\ \ \rangle$ here.

We now decompose our variables into a cross-sectional area-averaged component and a deviation component, as suggested by the work of Stone and Brenner [25] and Huber and Santiago [26]. In Cartesian coordinates, the decomposed variables take the form $\varphi(x,y) = \bar{\varphi}(x) + \varphi'(x,y)$, where $\bar{\varphi} = (\int \varphi dA)/A$ is the area-averaged value and the prime denotes the deviation component. Performing cross-sectional average of Eq. (1), products containing a single deviation term are eliminated by definition (the average of a deviation term is zero). As a result, Eq. (1) yields

$$\bar{u}\frac{\partial\bar{\theta}}{\partial x} = \alpha\left(\frac{\partial^2\bar{\theta}}{\partial x^2} + \frac{q(x)}{2Hk}\right) - \frac{\partial\left(\overline{u'\theta'}\right)}{\partial x} \tag{4}$$

where $q(x) = q_u(x) + q_b(x)$. As can be seen, the partial differential equation of Eq. (1) is now simplified to an ordinary differential equation which can be solved easier. It has the standard 1-D form of transport equation with the additional cross-correlation term that contributes to the heat dispersion. The average and deviation velocity terms appear in Eq. (4), are obtained from the following relationships [26]

$$\bar{u} = \frac{Q_{pd}}{H} + \frac{\mu_{eo,0}\Delta\mathrm{V}}{L}\frac{\langle\eta f g\rangle}{\langle\eta\rangle} \tag{5}$$

$$u' = \frac{1}{2}\left\{\frac{Q_{pd}}{H} + \frac{\mu_{eo,0}\Delta\mathrm{V}}{L}\left(\frac{\langle\eta f g\rangle}{\langle\eta\rangle} - f g\right)\right\}\left(1 - \frac{3y^2}{H^2}\right) \tag{6}$$

In order to determine the dispersion term in Eq. (4), another transport equation is required, which can be obtained by subtracting Eq. (4) from the decomposed form of Eq. (1)

$$\bar{u}\frac{\partial\theta'}{\partial x} + u'\frac{\partial\bar{\theta}}{\partial x} + u'\frac{\partial\theta'}{\partial x} - \overline{u'\frac{\partial\theta'}{\partial x}} = \alpha\left(\frac{\partial^2\theta'}{\partial x^2} + \frac{\partial^2\theta'}{\partial y^2} - \frac{q(x)}{2Hk}\right) \tag{7}$$

Under the assumption of $Pe_H(H/l) \ll 1, (H/l)^2 \ll 1\ and\ u' = O(u)$, Eq. (7) can be simplified to

$$\frac{\partial^2\theta'}{\partial y^2} = \frac{u'}{\alpha}\frac{\partial\bar{\theta}}{\partial x} + \frac{q(x)}{2Hk} \tag{8}$$

where the Peclet number is defined as follows $Pe_H = \bar{u}H(1 - u_{eo,0}fg/\bar{u})/\alpha$. Given an expression for u', the deviation term, θ' can be obtained in terms of the area-averaged temperature rise, $\bar{\theta}$ and heat flux, $q(x)$ by integration

$$\theta'(x,\xi) = \frac{A\xi^2(2-\xi^2)}{4}\frac{\partial\bar{\theta}}{\partial x} + \frac{B\xi(2+\xi)}{2} - \left(\frac{7A}{60} + \frac{B}{6}\right) \tag{9}$$

where A and B parameters can be obtained from the following relationships

$$A = \frac{H^2}{2\alpha}\left(\bar{u} - \frac{\mu_{eo,0}\Delta\mathrm{V}}{L}fg\right)$$
$$B = \frac{q(x)H}{2k} \tag{10}$$

and $\xi = y/H$ is the dimensionless distance from the center of the channel. We now use the solution of Eq. (9) to determine the advective dispersion contribution in Eq. (4)

$$\overline{u'\theta'} = -\frac{2Pe_H^2}{105}\alpha\frac{\partial\bar{\theta}}{\partial x} - \frac{Pe_H\alpha}{15k}q(x) \tag{11}$$

We substitute Eq. (11) into the averaged transport equation, Eq. (4), yielding the final form of

$$\bar{u}\frac{\partial\bar{\theta}}{\partial x} = \frac{\partial}{\partial x}\left(\alpha_{eff}\frac{\partial\bar{\theta}}{\partial x}\right) + \frac{\alpha q(x)}{2Hk}\left[1 + \frac{2Pe_H H}{15}\frac{q'(x)}{q(x)}\right] \tag{12}$$

where $q'(x) = dq(x)/dx$ and

$$\alpha_{eff} = \alpha\left(1 + \frac{2Pe_H^{\,2}}{105}\right) \tag{13}$$

The 1-D convection-diffusion of Eq. (12) has features of the Taylor-Aris dispersion equation. The thermal dispersion coefficient, α_{eff} accounts for the effects of the pressure driven flow on the area-averaged temperature. There is an additional term in Eq. (12) corresponds to the applied heat flux on the upper surface of the channel. This term can be more simplified under the following assumption

$$PeH\frac{q'(x)}{q(x)} \ll 1 \tag{14}$$

yielding

$$\bar{u}\frac{d\bar{\theta}}{dx} = \frac{d}{dx}\left(\alpha_{eff}\frac{d\bar{\theta}}{dx}\right) + \frac{\alpha q(x)}{2Hk} \tag{15}$$

Nondimensionalizing Eq. (14) with the assumption that α_{eff} remains constant gives

$$Pe_l\frac{\partial\bar{\theta}^*}{\partial x^*} = \frac{d^2\bar{\theta}^*}{dx^{*2}} + q^*(x) \tag{16}$$

subjected to the following boundary conditions

$$\bar{\theta}^*(x^* \to \pm\infty) = 0 \tag{17}$$

where $x = x^* l$, $\bar{\theta} = (q_0 l^2 \bar{\theta}^* / 2Hk)(\alpha/\alpha_{eff})$, $Pe_l = \bar{u} l / \alpha_{eff}$, and $q(x) = q_0 q^*(x)$. Note that, the boundary condition given in Eq. (17) is valid when channel length is much larger than the size of the heat source.

Thermal resistance analysis to the bottom (PMMA or glass substrates) and the top of the chip shows that the thermal resistance of the lower substrate can be effectively neglected in comparison with the free convection from the top and bottom surfaces. As a result,

We propose a solution, as an example, here for a microchannel that its upper surface is locally heated with a heat source of length l, with uniform heat flux and is cooled by free convection or conduction to the ambient. For such a condition, dimensionless heat flux can be written as follows

$$q(x)^* = \begin{cases} 1 - Bi\bar{\theta}^*; & -1 < x^* < 1 \\ -Bi\bar{\theta}^*; & x^* < -1 \; and \; 1 < x^* \end{cases} \quad (18)$$

where the Biot number is defined as $Bi = (hl^2/2Hk)(\alpha/\alpha_{eff})$. The solution of Eq. (18) has the following form

$$\bar{\theta}^* = \begin{cases} \dfrac{2m_1 \sinh(m_2)\, e^{m_2 x^*}}{(m_1 - m_2)Bi}; & x^* < -1 \\ \dfrac{1}{Bi} + \dfrac{m_2 e^{m_1(x^*+1)} - m_1 e^{m_2(x^*-1)}}{(m_1 - m_2)Bi}; & -1 < x^* < 1 \\ \dfrac{2m_2 \sinh(m_1)\, e^{m_1 x^*}}{(m_1 - m_2)Bi}; & 1 < x^* \end{cases} \quad (19)$$

where the new parameters are $m_1 = \left(Pe_l - \sqrt{4Bi + Pe_l^2}\right)/2$ and $m_2 = \left(Pe_l + \sqrt{4Bi + Pe_l^2}\right)/2$.

One limiting case for the solution proposed in Eq. (19) is when $Pe_l \to 0$. For such a problem heat transfer occurs only through conduction and the convective term in Eq. (16) is negligible. As a result, Eq. (19) simplifies to

$$\bar{\theta}^* = \begin{cases} \dfrac{e^{-\sqrt{Bi}x^*} \sinh(Bi)}{Bi}; & x^* < -1 \\ \dfrac{2 - e^{-\sqrt{Bi}(x^*+1)}\left(1 + e^{2\sqrt{Bi}x^*}\right)}{2Bi}; & -1 < x^* < 1 \\ \dfrac{e^{\sqrt{Bi}x^*} \sinh(Bi)}{Bi}; & x^* < -1 \end{cases} \quad (21)$$

For very high velocities, convection dominates the heat transfer mechanism, yielding very small temperature rise in the fluid. As a result, $\bar{\theta}^* \to 0$.

4. RESULTS AND DISCUSSION

In order to determine the performance of the proposed optothermal heating approach in controlling the temperature of a liquid sample in the microfluidic system, effects of different controlling parameters are investigated here.

Figure 3 is the experimental demonstration of the proposed heating system ability to control the location of the heated area. The heat source location was controlled only by the image generated (and sent to the projector) from an external computer. Because the channel depth is much smaller than the channel width, the temperature difference in the depth direction is small and the monitored 2D fluorescence accurately represents the temperature field of the fluid within the microchannel. As can be seen, temperature gradient up to 35 ℃ can be achieved by a 1.5 mm heat source. This temperature gradient is suitable for many microfluidic applications such as patch-clamp electrophysiology [2], rheological flow manipulation [7], polymer actuators [8], and temperature gradient focusing [4].

Figure 4 presents the variation of maximum temperature rise along the microchannel with the heat source width. The results are obtained for no flow condition. The width and maximum temperature rise are normalized with respect to the width and maximum temperature rise of the heat source of 1.5 mm width. As expected, since more heat is transferred to the fluid, maximum temperature increases with the source width in a linear behavior.

In order to control the applied heat flux, we changed the light intensity by adjusting the darkness of the rectangular strip projected from the external computer. Figure 5 shows the variation of normalized temperature rise for different applied heat fluxes when the source size was kept constant. The fairly linear behavior of the results suggests that the heat flux changes proportionally with the light intensity in a linear manner. It should be noted that the results in Figure 5 are plotted for no flow condition.

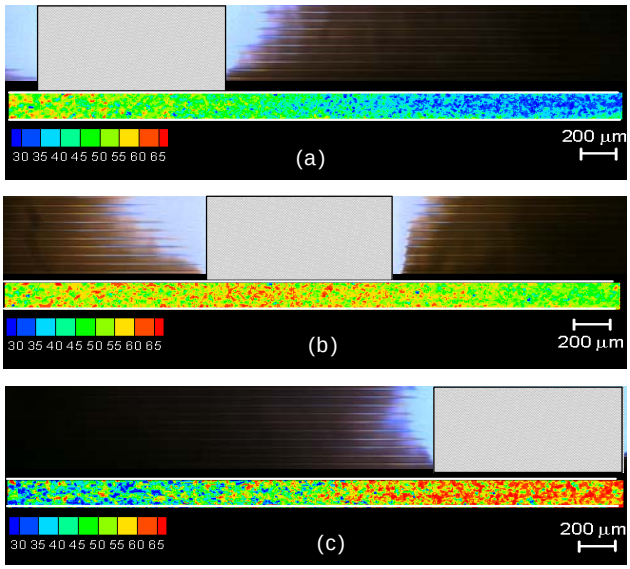

Figure 3. Experimental demonstration of localized heating with the optothermal system. The microchannel was heated at three different locations, (a, b and c), with a heat source of approximately 1.5 mm width. Total field of view for each image is 3.5 mm. Images were taken for no flow condition while the heat source location was controlled by that projected from an external computer. In each image, the top pane is an image produced by the video projector and the lower pane shows the corresponding temperature contour.

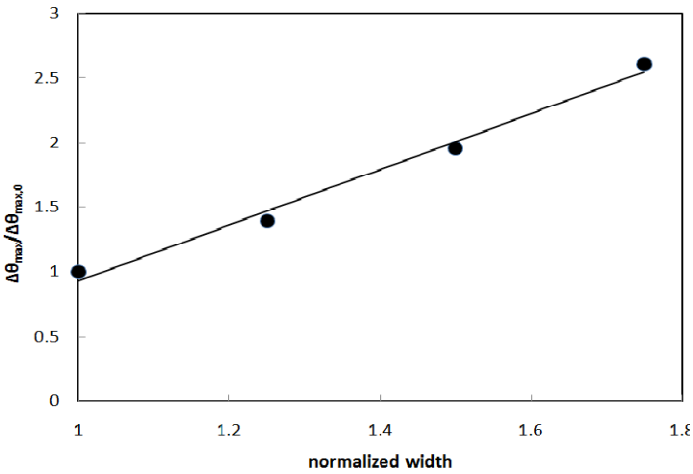

Figure 4. Effect of the source width on the maximum temperature rise within the microchannel for no flow condition. The width and maximum temperature rise are normalized with respect to the reference width of 1.5 mm. Filled circles are the experimental data and the solid line is a linear fit.

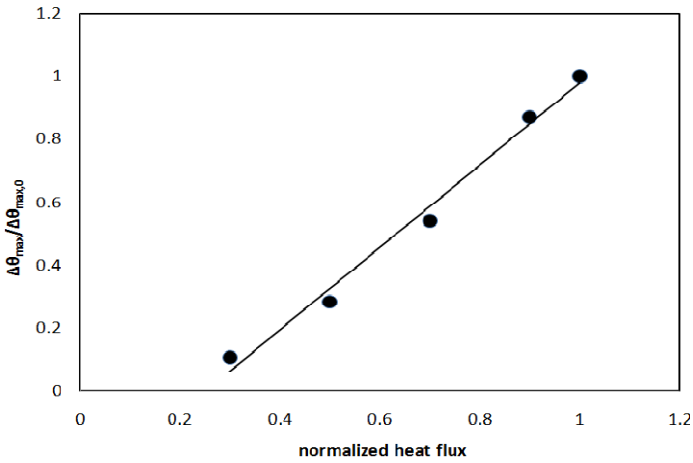

Figure 5. Variation of normalized maximum temperature rise versus applied heat flux. The heat source width was kept constant with the value of 1.5 mm. The intensity of the light was controlled by adjusting the darkness of the image. Filled circles are the experimental data and the solid line is a linear fit.

In order to investigate the effects of fluid velocity on the temperature field, variation of temperature distribution along the microchannel for different Peclet numbers is shown in Figure 6. The measured temperature at each axial location is obtained by cross-sectional averaging of the temperature. To compare the temperature distribution in the presence of fluid flow with the proposed theoretical model, the no flow condition experimental result is used as a benchmark to set the heat flux in the analytical model. Values of the parameters used in the theoretical model are listed in Table 1. Afterward, the same heat flux is used to compute the temperature distribution in the presence of fluid velocity. Note that calculation of maximum length scale for the system according to [26] shows that the Reighley number is always small enough that free convection from the upper and lower surfaces can be neglected and heat conduction in the air is the only mechanism heat transfer. As a result, we considered the conductive process as a heat source within a half-space and the values obtained by [29] were used to estimate the equivalent free convection coefficient (i.e. h).

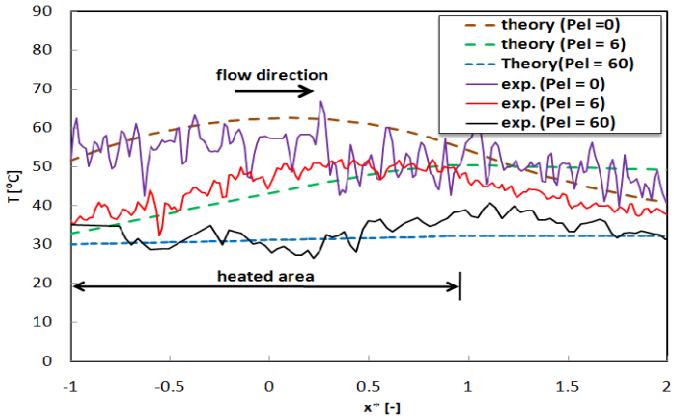

Figure 6. Variation of temperature distribution along the channel for different fluid velocities. Experimental temperature at each axial location is obtained by cross-sectional averaging of the temperature. Source width is kept constant with the value of 1.5 mm.

It can be seen that the simple theoretical model can predict the trend in the experimental data. In particular, both theoretical and experimental data show that the maximum temperature decreases when the fluid velocity (or Pe_l) increases. This is expected as given a constant heat flux, the temperature change decreases as the mass flow rate of fluid increases. It is also clear from the plot that the location of the maximum temperature shifts from the center of the heat source to the downstream of the flow by increasing the fluid velocity. This can be attributed to the fact that more cold fluid is pumped under the heat source and cools the front edge of the heat source..

5. CONCLUSION AND RECOMMENDATIONS

We present an optothermal heating for microfluidic flow that enables dynamic control of the heated location and intensity, using a commercial video projector and an optical deliver system. The proposed system provides heating up to 35℃ over ambient temperature for a heat source size of 1.5 mm which can be used in many microfluidic applications.

The heat source size, location and intensity can be controlled from an external computer using common user interface software such as Microsoft Power Point or Matlab. According to the obtained experimental data the following were observed:

- Increasing the source width leads to increase in the maximum temperature within the microchannel. This increase is linearly related to the source width.
- Source heat flux is related in a linear manner to the darkness of the generated image.
- The amount of maximum temperature decreases when the fluid velocity increases.
- The location of the maximum temperature is almost under the center of the heat source for no flow condition and it shifts from the center of the heat source to the downstream of the flow by increasing the fluid velocity.

Table 1. Values of the parameters used in the theory for comparison with experimental data.

Parameter	Value
l	$0.75\ mm$
H	$10\ \mu m$
q	$1250\ W/m^2$
k	$0.54\ W/m.K$
ρ	$1000\ kg/m^3$
c_p	$4200\ J/kg.K$
h	$15\ W/m^2K$

A simple 1D analysis was introduced for better understanding of the thermal behavior of the system in the presence of the fluid flow. The closed form solution is obtained for cross-sectional average of the temperature in terms of fluid velocity. Given the thermal properties, source width, channel height, and convective/conductive heat transfer coefficient to ambient, the analysis shows good agreement with the experimental data. Effects of all the following parameters were considered in three dimensionless parameters: Pe_H, Pe_l and Bi.

Although the present heating system is applicable to the proposed optothermal system the heat source size should be shrunk down more to provide higher resolutions in the temperature control of the system. For future works, the capacity to move the heat sources with rapid heating and cooling rates will be examined and compared with the modified theoretical analysis for a transient condition. The present system will also be employed in to manipulate analytes using the pre-concentration method of Temperature gradient focusing.

ACKNOWLEDGMENTS

The authors gratefully acknowledge the financial support of the Natural Sciences and Engineering Research Council of Canada, NSERC.

REFERENCES

[1] Watts, P, An Chemical synthesis in micro reactors, Chemie Ingenieur Technik 76 (2004) 555–559.
[2] Pennel T., Suchyna T., Wang, j., Heo, J., Felske, J., Sachs, F., and Hau, S., Microfluidic microchip to produce temperature jumps for electrophysiology, Anal. Chem. 80 (2008) 2447-2451.
[3] Zhang, C., Xu, J., Ma, W., and Zheng, W., PCR microfluidic devices for DNA amplification, Biotechnology Advances 24 (2006) 243-284.
[4] Ross, D. and Locascio, L.E., Microfluidic temperature gradient focusing, Anal. Chem. 74 (2002) 2556-2564.
[5] Sommer, G.J., Kim, S.M., Littrel, R.J., and Hasselbrink, E.F., Theoretical and numerical analysis of temperature gradient focusing via joule heating, Lab on a Chip 7(2007) 898-907.
[6] Duhr, S. and Braun, D., Why molecules move along a temperature gradient, PNAS 103(52) (2006) 19678-19682.
[7] Krishnan, M., Oark, J., and Erickson, D., Optothermorheological flow manipulation, Optics Letters 34 (13) (2009) 1976-1978.
[8] Richter, A. and Paschew, G., Optoelectrothermic control of highly integrated polymer-Based MEMS applied in an artificial skin, Advanced Materials 21 (2009) 979-983.
[9] Yang, H., Choi, C.A., Chung, K.H., Jun, C.H., and Kim Y.T., An independent temperature-controllable microelectrode array. Anal. Chem. 76 (5) (2004) 1537– 43.
[10] Kaigala, G. V., Hoang, V. N., Stickel, A., Lauzon, J., Manage, D., Pilarski, L. M., and Backhouse, C. J., An inexpensive and portable microchip-based platform for integrated RT–PCR and capillary electrophoresis, Analyst 133 (2008) 331–338.
[11] Liao, C.S., Lee, G.B., Wu, J.J., Chang, C.C., Hsieh, T.M., and Huang, F.C., Micromachined polymerase chain reaction system for multiple DNA amplification of upper respiratory tract infectious diseases, Biosens Bioelectron 20 (2005) 1341–1348.
[12] Fu, R., Xu, B., and Li, D., Study of the temperature field in microchannels of a PDMS chip with embedded local heater using temperature-dependent fluorescent dye, Int. J. Thermal Science 45 (2006) 841-847.
[13] Liu, Y., Rauch, C. B., Stevens, R. L., Lenigk, R., Yang, J., Rhine, D. B. , and Grodzinski, P., DNA Amplification and Hybridization Assays in Integrated Plastic Monolithic Devices, Anal. Chem. 74 (2002) 3063–3070.
[14] Lee DS, Park SH, Yang H, Chung KH, Yoon TH, Kim SJ, Bulk micromachined submicroliter-volume PCR chip with very rapid thermal response and low power consumption, Lab Chip 4 (2004) 401–407.
[15] Wang, Q., Tan, Y., Gong, H., An integrated system for real-time PCR analysis based on microfluidic biochip, Int. J. Comp. Eng. Sci. 4(2) (2003) 285 –288.
[16] Oda, R.P., Strausbauch, M.A., Huhmer, A.F.R., Borson, N., Jurrens, S.R., and Craighead, J., Infrared-mediated

thermocycling for ultrafast polymerase chain reaction amplification of DNA, Anal. Chem. 70 (1998) 4361– 4368.
[17] Ke, C., Berney, H., Mathewson, A., Sheehan, M.M., Rapid amplification for the detection of Mycobacterium tuberculosis using a non-contact heating method in a silicon microreactor based thermal cycler, Sensors and Actuators B 102(2) (2004) 308-314.
[18] Issadore, D. , Humphry, K. J., Brown, K. A., Sandberg, L., Weitz, D. A., and Westervelt, R. M., Lab Chip 9 (2009) 1701–1706.
[19] Guijt, R.M., Dodge, A., van Dedem, G.W.K., de Rooij, N.F., and Verpoorte, E., Chemical and physical processes for integrated temperature control in microfluidic devices, Lab Chip 3 (2003) 1–4.
[20] Vigolo, D., Rusconi, R., Piazzaa, R., and Howard A., Stone, A., portable device for temperature control along microchannels, Lab Chip 10 (2010) 795-798.
[21] Erickson, D., Sinton, D., Li, D., Joule heating and heat transfer in poly(dimethylsiloxane) microfluidic systems, Lab-on-a Chip 3 (2003) 141-149.
[22] Liu, G.L., Kim, J., Lu, Y., and Lee, L.P., Optofluidic control using photothermal nanoparticles, Nature materials 5 (2005) 27-32.
[23] Reinhardt,H., Dittrich, P.S., Manz, A., and Franzke, J., μ-Hotplate enhanced optical heating by infrared light for single cell treatment, Lab Chip 7 (2007) 1509-1514.
[24] Grouselle, M., Tuex, O., Dabadie, P., Georgescaud, D., and Mazat, J., Effect of local anaesthetics on mitochondrial membrane potential in living cells, J. Biochem. 271 (1990) 269-272.
[25] Ghosal, S. and Horek, J., Mathematical model describing gradient focusing methods for trace analytes, Anal. Chem. 77 (2005) 5380–5384
[26] Huber, D. and Santiago, J.G., Taylor–Aris dispersion in temperature gradient focusing, Electrophoresis 28 (2007) 2333-2344.
[27] Stone, H.A. and Brenner, H., Dispersion in Flows with Streamwise Variations of Mean Velocity: Radial Flow, Ind. Eng. Chem. Res. 38 (1999) 851-854.
[28]Bejan, A., Convection Heat Transfer, 3rd Ed., (2004), John Wiley and Sons Inc., NJ.
[29] Yovanovich, M. M., Burde, S. S., and Thompson, J. C., 1977, Thermal Constriction Resistance of Arbitrary Planar Contacts with Constant Heat Flux, AIAA Progress in Astronautics and Aeronautics: Thermophysics of Spacecraft and Outer Planet Entry Probes, 56, A. M. Smith, ed., pp. 127–139.
[30] D. Ross, T. J. Johnson and L. E. Locascio, Temperature measrument in microfluidic systems using a temperature dependent fluorescent dye, Anal. Chem. 73 (2001) 2509–2515.